

# Remotely induced magnetism in a normal metal using a superconducting spin-valve

M. G. Flokstra<sup>1\*</sup>, N. Satchell<sup>2</sup>, J. Kim<sup>2</sup>, G. Burnell<sup>2</sup>, P. J. Curran<sup>3</sup>, S. J. Bending<sup>3</sup>, J. F. K. Cooper<sup>4</sup>, C. J. Kinane<sup>4</sup>, S. Langridge<sup>4</sup>, A. Isidori<sup>5</sup>, N. Pugach<sup>5,6</sup>, M. Eschrig<sup>5</sup>, H. Luetkens<sup>7</sup>, A. Suter<sup>7</sup>, T. Prokscha<sup>7</sup> and S. L. Lee<sup>1</sup>

**Superconducting spintronics has emerged in the past decade as a promising new field that seeks to open a new dimension for nanoelectronics by utilizing the internal spin structure of the superconducting Cooper pair as a new degree of freedom<sup>1,2</sup>. Its basic building blocks are spin-triplet Cooper pairs with equally aligned spins, which are promoted by proximity of a conventional superconductor to a ferromagnetic material with inhomogeneous macroscopic magnetization<sup>3</sup>. Using low-energy muon spin-rotation experiments we find an unanticipated effect, in contradiction with the existing theoretical models of superconductivity and ferromagnetism: the appearance of a magnetization in a thin layer of a non-magnetic metal (gold), separated from a ferromagnetic double layer by a 50-nm-thick superconducting layer of Nb. The effect can be controlled either by temperature or by using a magnetic field to control the state of the remote ferromagnetic elements, and may act as a basic building block for a new generation of quantum interference devices based on the spin of a Cooper pair.**

The ability to manipulate the spin degree of freedom of charge carriers is key to realizing future spin-based electronics. Integrating superconductors into spintronic devices can greatly enhance performance<sup>1</sup> and allows the transport of spin over long distances without the dissipation of heat<sup>2</sup>. To achieve the alignment of electron spins, ferromagnetic materials are used. Superconductivity and ferromagnetism are, however, antagonistic states of matter, and the interplay between these two states results in the conversion of conventional spin-singlet into spin-triplet pair correlations<sup>3</sup>. Whereas spin-singlet pairs have spin angular momentum  $S=0$ , spin-triplet pairs have  $S=1$ , with three possible spin projections  $s_z = -1, 0, +1$ . The realization of such spin-triplet pairs in mesoscopic systems containing interfaces between superconducting (S) and ferromagnetic (F) layers has attracted much interest from both the theoretical and experimental communities. Interaction of spin-singlet superconductivity with collinear ferromagnetism leads to oscillations and suppression of the pair correlation at a short distance  $\xi_f$  due to the exchange magnetic field in the ferromagnet, which tends to align the spins of electrons parallel<sup>4–7</sup>. However, to create longer-range penetration of spin-triplet superconductivity into the ferromagnet, interaction with a non-collinear magnetism is required<sup>8–10</sup>, motivating the discovery of superconducting currents through ferromagnetic metals over distances far longer than the singlet penetration length

$\xi_f$  (refs 11–13). These long-range triplet components (LRTC) have parallel spin projections ( $s_z = \pm 1$ ), and are not suppressed by the exchange field. Theory predicts that the conversion into spin-triplet pairs should also give rise to an induced magnetic moment in the superconductor, decaying away from the interface<sup>14–16</sup>, often called the inverse or magnetic proximity effect. For diffusive systems this induced magnetic moment is predicted to be negative (opposite to the magnetization of itinerant electrons in the adjacent F layer) and accompanied by a small decrease of magnetization of this F layer on the scale of the ferromagnetic coherence length  $\xi_f$ . There are a small number of reports with observations that are attributed to this effect<sup>17–19</sup>, although none use a measurement technique that has the required spatial sensitivity to uniquely determine this. A further report involving low-energy muon spin-rotation (LE- $\mu$ SR) measurements, a technique possessing the required spatial sensitivity to determine the location of the moment, found contradictory evidence<sup>20</sup>. The moment was found not to penetrate into the S layer over the expected distance of a coherence length, but rather it existed over a very much shorter length scale, indicating a rather different interfacial mechanism at play in that system, and possibly also in related works.

Here we report results obtained by high-precision LE- $\mu$ SR that are in conflict with the current theoretical predictions, and which yield instead a very surprising, hitherto unknown effect. We find a switchable magnetic moment to be induced remotely from the superconductor–ferromagnet interface, at a non-magnetic superconductor–normal metal interface about 150 atomic layers away from the ferromagnet. The moment appears, however, not inside the S layer, but in an adjacent normal metal (N) layer. It first appears at the onset of superconductivity and increases as the temperature is lowered. This remote induced magnetic moment also exhibits a spin-valve effect: a significant change in magnitude ( $\sim 20$  times) depending on the mutual orientation of magnetization in the F layers in the NSFF multilayered structure. The effect almost disappears when switching the spin-valve into a collinear state of the F layers' magnetization, when LRTC are absent. This shows that LRTC in the ferromagnetic regions are a crucial ingredient contributing to the effect.

For our experiments we use superconducting spin-valve structures Au( $x$ )/Nb(50)/Co(2.4)/Nb(3)/Co(1.2)/IrMn(4)/Co(3)/Ta(7.5)/Si-substrate with numbers indicating the layer thicknesses in nm and  $x = 5$  or 70. They consist of an S/F interface with an

<sup>1</sup>School of Physics and Astronomy, SUPA, University of St Andrews, St Andrews KY16 9SS, UK. <sup>2</sup>School of Physics and Astronomy, University of Leeds, Leeds LS2 9JT, UK. <sup>3</sup>Department of Physics, University of Bath, Claverton Down, Bath BA2 7AY, UK. <sup>4</sup>ISIS, Rutherford Appleton Laboratory, Oxfordshire OX11 0QX, UK. <sup>5</sup>SEPnet and Hubbard Theory Consortium, Department of Physics, Royal Holloway, University of London Egham, Surrey TW20 0EX, UK. <sup>6</sup>Skobel'syn Institute of Nuclear Physics, Lomonosov Moscow State University (SYNP MSU), Leninskie Gory, Moscow 119991, Russia. <sup>7</sup>Labor für Myonspinspektroskopie, Paul Scherrer Institut, CH-5232 Villigen PSI, Switzerland. \*e-mail: [mgf@st-andrews.ac.uk](mailto:mgf@st-andrews.ac.uk)

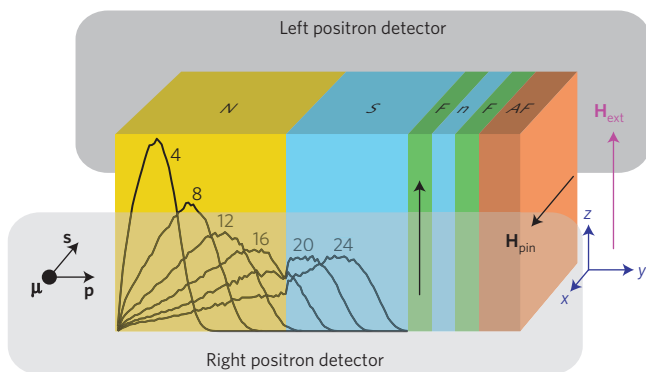


**Figure 1 | Sample architecture and experimental arrangement.** Schematic of the sample architecture (NSFnF), centred between the positron detectors within a homogeneous applied field ( $H_{\text{ext}}$ ) along the  $z$ -direction. The momentum ( $\mathbf{p}$ ) of the incoming muon ( $\mu$ ) is normal to the sample plane (along the  $y$ -direction) and its initial spin ( $\mathbf{s}$ ) points towards the left positron detector. The direction of the exchange field of the (free) F layer closest to the S layer is saturated along the applied field direction, whereas the second (pinned) F layer is always directed along the pinning direction from the anti-ferromagnet ( $H_{\text{pin}}$ ). The sample orientations used were either with  $H_{\text{pin}}$  aligned with  $H_{\text{ext}}$  (collinear arrangement) or perpendicular to it (orthogonal arrangement). Muon stopping profiles are overlaid on the front face of the sample to indicate the probability distribution for muons with increasing energies between 4 and 24 keV with 4 keV steps. The higher the energy the further the muons penetrate on average into the sample, but this also broadens the profile. Up to 12 keV all muons stop within the N layer and only for higher energies does an increasing fraction stop within the S layer.

additional N layer atop the S, as well as a second F layer separated from the first by a thin normal metal spacer (n), creating a NSFnF device, shown schematically in Fig. 1 (see Supplementary Information for more details of our spin-valves). In our devices the exchange field of the outer F layer (Co(1.2)) can be pinned magnetically, by using an anti-ferromagnet (IrMn), while retaining easy manipulation of the other F layer (Co(2.4)). This enables us to control the angle between the two F magnetizations and thus explore the inverse proximity effect in both the orthogonal configuration as well as the collinear configuration. In other words, to examine the (possible) induction of magnetic moments when the LRTC are present (non-collinear configuration) and compare it with the case where they are absent (collinear configuration). A dependence of  $T_c$  on the magnetic configuration in such structures has been proposed<sup>21</sup> and measured<sup>22–24</sup>. For the case of a strongly spin-polarized ferromagnet, owing to the appearance of the new LRTC channel for drainage of Cooper pairs from the S to the F layers, the change of  $T_c$  between the collinear and perpendicular configuration may be much more pronounced than between parallel and antiparallel alignment<sup>24</sup>.

To study the flux profile  $B(y)$  as a function of depth  $y$  in our superconducting spin-valves we use LE- $\mu$ SR at low temperatures (3–10 K). During a muon experiment, low-energy spin-1/2 muons ( $\sim 4$ –26 keV) are implanted into the sample at normal incidence to the sample surface. The actual implantation profile depends on the muon energy (see Fig. 1) and can be accurately calculated using Monte Carlo simulations<sup>25</sup>. Once implanted, the muon spin starts to precess around the local field direction with a frequency that is proportional to the local field strength, before it eventually decays and emits a positron preferentially along its momentary muon spin direction, allowing the time evolution of the muon spin to be monitored. LE- $\mu$ SR is an exquisitely sensitive technique with which to determine the local flux density with a spatial resolution better than the coherence lengths involved. A series of measurements are made, varying the implantation energy (average implantation depth) at

fixed temperatures. This allows a comparison of the flux profile  $B(y)$  obtained above and below the superconducting transition temperature to study the remote proximity effect and demonstrate its connection to superconductivity. A typical approach to fitting the muon data for a particular implantation energy is to use standard model functions characterized by the average flux  $\langle B \rangle$  across that stopping profile<sup>25</sup>. Repeating this for a range of implantation energies, each corresponding to a different average depth ( $y$ ) into the sample, provides a good indication of the spatial dependence of  $\langle B \rangle(y)$ . A more sophisticated approach to modelling involves combining information from all implantation energies and fitting simultaneously to a common  $B(y)$  describing the actual flux profile across the sample depth<sup>24</sup> while taking into account the full stopping profiles of the muons.

The main results of the analysis of our LE- $\mu$ SR data are presented in Fig. 2a. The induced magnetic profile  $B(y)$  is presented as a function of position for orthogonal and collinear arrangements, determined both above ( $T = 10$  K) and below ( $T = 3$  K) the superconducting transition temperature ( $T_c \sim 7.5$  K). Above  $T_c$  the magnetic profile obtained, for both arrangements, is approximately constant at the external field of 150 G. However, on cooling to below  $T_c$  a sudden appearance of a magnetic induction in the Au layer is obtained for the orthogonal arrangement, which almost completely disappears in the collinear arrangement (in our experiments we probe the parallel aligned collinear state). This startling result is independent of any modelling: for energies below 12 keV the muons stop entirely within the Au layer and the net magnetization averaged across that layer is unambiguously determined (Fig. 2b). Furthermore, inside the superconductor no observable change is detected for either magnetic state, thus indicating that the Meissner screening is unobservably small. This is consistent with earlier findings<sup>20</sup>, reflecting both the thinness of the superconducting layer and the strong suppression of the superconducting order parameter by proximity to ferromagnetism. Figure 2b shows a comparison between both types of modelling, where the  $\langle B \rangle(y)$  obtained for each individual data set (square symbols) are compared to the calculated values from the results shown in Fig. 2a (solid lines). The generally good agreement shows the obtained  $B(y)$  is indeed a good representation of the actual magnetic profile (see Supplementary Information for more details of alternative fitting functions). When comparing the behaviour in the superconducting and normal states, the results can be summarized as follows. A magnetization is induced in the normal metal with a sign opposite to the magnetization direction of the free F layer (as it subtracts from the applied field of 150 G), which decays away towards the surface of the sample on a scale  $\sim 20$  nm. This effect is clearly visible in the orthogonal arrangement, but diminishes (by a factor of 20) for the collinear arrangement. Unexpectedly, no induced magnetization is observable in the superconducting layer. All these facts are inconsistent with the theory<sup>14–16</sup> of the inverse (magnetic) proximity effect.

The temperature dependence of this effect, which disappears above  $T_c$ , shows a clear correlation with the model-independent measurement of the average moment in the Au at the onset of superconductivity (see Fig. 2c). This demonstrates that the S layer, itself not being spin-polarized, nevertheless provides this nonlocal magnetic effect. To further examine this absence of induced moment in the superconductor we measure a sample with a much thinner (5 nm) normal metal cap, but otherwise identical to the sample from Fig. 2a, in the orthogonal arrangement. This allows the superconductor layer to be probed directly without mixing in a large contribution from the N cap. No difference in the field profiles with temperature is observed for muon energies that probe the sample up to the interface with the F layer (see Fig. 3). This provides the final independent confirmation of the aforementioned three key observations embodied in the global fits of the flux profile. Nevertheless, a small contribution of an additional positive

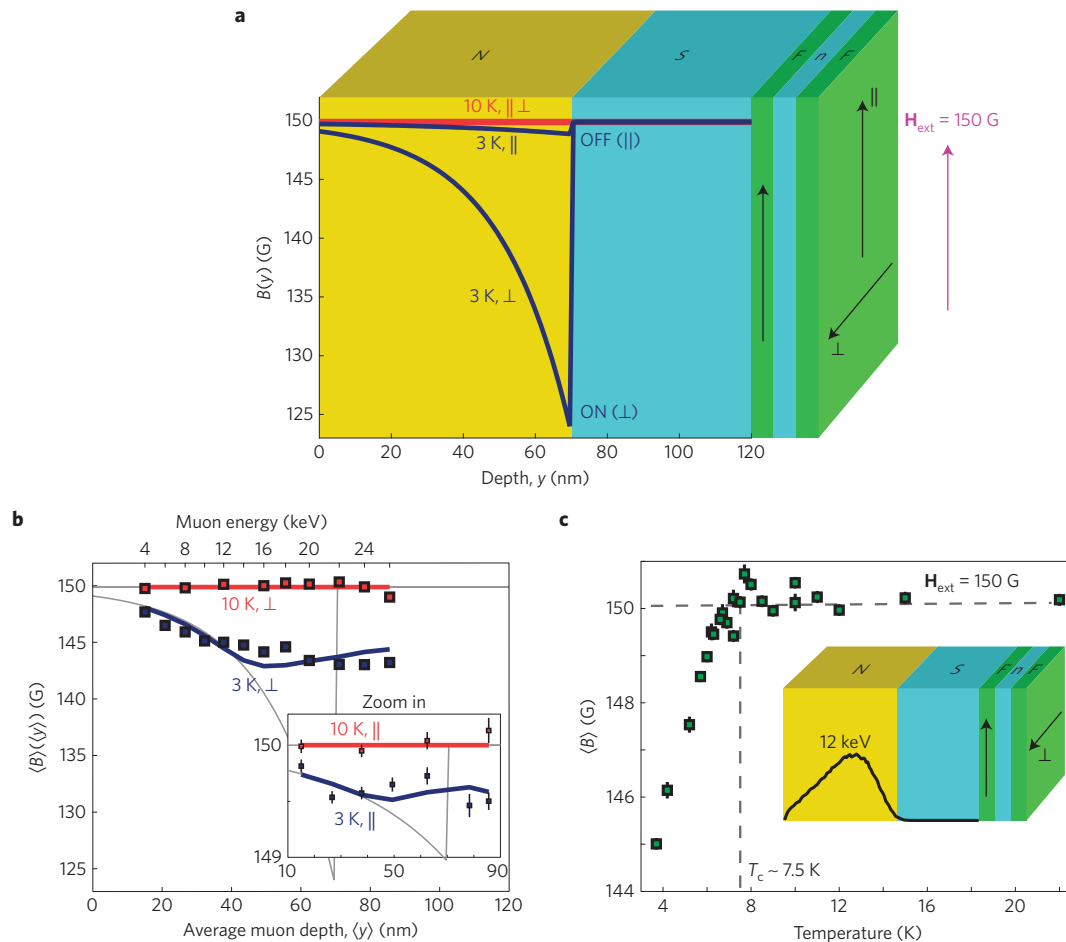


**Figure 2 | Fit results to LE- $\mu$ SR data on the NSF/F architecture.** **a**, Magnetic flux profile  $B(y)$  obtained from fitting all data simultaneously (at fixed temperature), for both the collinear ( $\parallel$ ) and orthogonal ( $\perp$ ) arrangement. Red for  $T=10$  K and blue for  $T=3$  K. For the latter an exponentially decaying model function was used whereas the former is taken to be constant. **b**, Average magnetic flux  $\langle B \rangle(y)$  obtained from fitting each data set individually (that is, the conventional treatment) compared to the calculated values from the profiles of **a**. Top axis shows the corresponding muon energies of the data points. **c**, Temperature dependence of the average flux  $\langle B \rangle$  in the orthogonal arrangement, taken at a muon energy of 12 keV (muon stopping profile shown in inset) to ensure all muons stopped in the Au layer. In **b** and **c**, the error bars indicate the asymptotic standard error in  $\langle B \rangle$ .

magnetization (along the external magnetic field) was detected at the highest muon energy, where muons also stop in the F/F region, which thus contributes to the signal.

Current theories do not account for our observed effect, and two main facts require explanation: the remote magnetization provided by superconductivity of the interlayer, and its dependence on the mutual orientation of the F layers' magnetization. Here we propose potential mechanisms to understand these results (see Supplementary Information for further details). The first question to address is how a thick superconducting layer, itself not being magnetized, may provide the transfer of magnetization (or spin polarization) from the F/F region to the N layer. We envisage two possibilities: the first being spin transfer by crossed Andreev reflection (CAR) and elastic co-tunnelling (EC; ref. 26) and the second being spin transfer by pure spin currents. The former involves spin-singlet pairs either being formed from electrons originating from the interfaces at opposite sides of the S layer (CAR) or being used to effectively transfer an electron from one of the interfaces to the other interface (EC). The alternative involves flows of spin-triplet pairs (and is thus a direct consequence of having LRTC in the system) where a net flow of spin-up electron pairs moving from one side of the S layer to the other side is cancelled by an opposing flow of spin-down electron pairs. These mechanisms are illustrated in Fig. 4 for the case of a spontaneous spin accumulation in the F/F region, where,

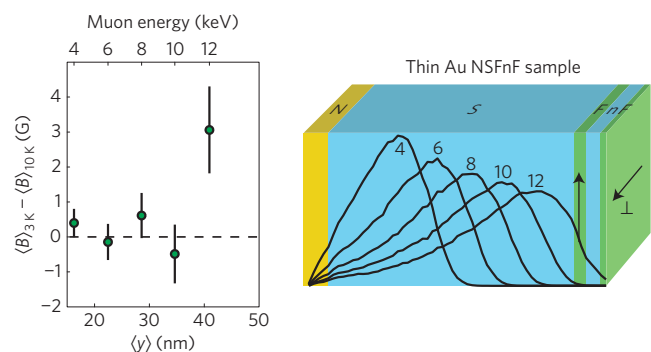


**Figure 3 | Thin Au cap sample.** Difference between the induced magnetic flux at  $T=3$  K and that at  $T=10$  K, with error bars indicating the asymptotic standard error in  $\langle B \rangle_{3K} - \langle B \rangle_{10K}$ , for the NSF/F architecture with a very thin 5 nm N (Au) cap in the orthogonal arrangement (shown with muon stopping profiles overlaid on the front face). The highest energy (12 keV) includes contributions from the n-spacer. It is only in the region of the F/F interface that any difference is detected between above and below  $T_c$ .

for illustration purposes, the spin accumulation is represented by a chemical potential shift between the spin-up and spin-down bands, but should be imagined as a proximity-induced imbalance between

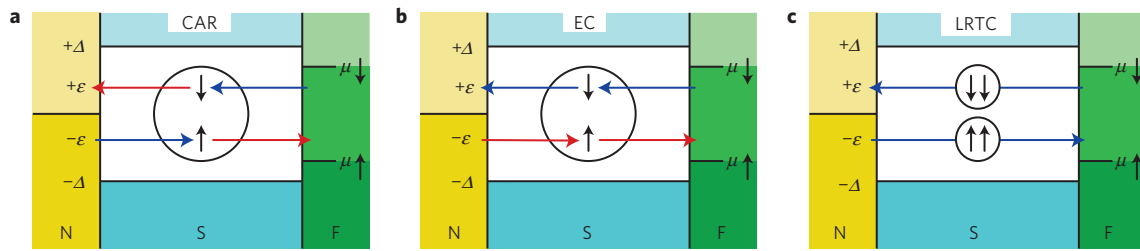


**Figure 4 | Spin-transfer mechanisms.** Schematic of the proposed mechanisms to transfer spin across the superconductor (S) with gap energy  $\Delta$  when there is a spin accumulation in the ferromagnet (F) resulting in a shift between the chemical potentials  $\mu$  of the spin-up and spin-down band. **a**, During a crossed Andreev reflection (CAR) a singlet Cooper pair (CP) is created from an electron at energy  $+\varepsilon$  with spin down ( $+\varepsilon_{\downarrow}$ ) originating from the F layer and an electron at energy  $-\varepsilon$  with spin up ( $-\varepsilon_{\uparrow}$ ) originating from the normal metal (N) layer (blue arrows). CAR can also annihilate a CP by donating electron  $+\varepsilon_{\downarrow}$  into the N and  $-\varepsilon_{\uparrow}$  into the F layer (red arrows). **b**, During an elastic co-tunnelling (EC) process a singlet CP attracts electron  $+\varepsilon_{\downarrow}$  from the F layer while simultaneously donating its own  $+\varepsilon_{\downarrow}$  electron into the N layer (blue arrows). EC can also attract electron  $-\varepsilon_{\uparrow}$  from the N layer and donate its own electron  $-\varepsilon_{\uparrow}$  into the F layer (red arrows). **c**, A flow of polarized (triplet) Cooper pairs can transfer spin across the S layer, without generating a moment inside the S layer. Triplet pairs of  $+\varepsilon_{\downarrow}$  electrons move from the F to the N layer while an equal flow of triplet pairs of  $-\varepsilon_{\uparrow}$  electrons move from the N to the F layer.

up and down spins due to broken particle-hole symmetry of the spin-resolved density of states<sup>27</sup>.

The second question to address is the observed spin-valve effect: the disappearance of the remote magnetization together with the LRTC at the collinear magnetic configuration. To transfer the observed negative magnetization into the N layer by the CAR or EC mechanism, some negative spin accumulation must exist near the S/F interface. Spin accumulation itself appears as a result of spin current decay<sup>28</sup> (it could also be ascribed to the inverse proximity effect<sup>14</sup>, but, as that would not result in spin-valve behaviour, we exclude it as a candidate mechanism). It was shown that spin currents, both normal<sup>29</sup> and superconducting<sup>30,31</sup>, appear in FNF spin-valves with non-collinear spin alignment (where LRTC are present), even in an unbiased structure, but disappear in the collinear geometry (where LRTC are absent). Thus spontaneous spin currents in the FNF region can lead to spin accumulation in the N layer by CAR and EC processes. The existence of spontaneous spin accumulation have also been reported in a Josephson junction between a spin-singlet and a spin-triplet superconductor<sup>27</sup> and in an S/F/S Josephson junction with strong spin-orbit coupling in the F layer<sup>32</sup>.

Separating spin and charge currents and generating spin-polarized electron populations are the key building blocks of spintronics. Our experiments demonstrate the spontaneous long-distance transfer of magnetization across a superconductor to a normal metal without the involvement of charge current, temperature gradient or driving voltage. Our results further demonstrate that the effect is attributable to spin-triplet superconducting correlations induced in a non-collinear FNF-trilayer, disappearing for a collinear arrangement. It provides a mechanism by which dissipation-less superconducting spintronic devices might be realized. This unexpected and theoretically unanticipated effect requires further experimental and theoretical work for a detailed understanding.

## Methods

Methods and any associated references are available in the [online version of the paper](#).

Received 15 May 2015; accepted 21 August 2015;  
published online 5 October 2015

## References

- Linder, J. & Robinson, J. W. A. Superconducting spintronics. *Nature Phys.* **11**, 307–315 (2015).
- Eschrig, M. Spin-polarized supercurrents for spintronics. *Phys. Today* **64**(1), 43–49 (2011).
- Buzdin, A. I. Proximity effects in superconductor–ferromagnet heterostructures. *Rev. Mod. Phys.* **77**, 935–976 (2005).
- Jiang, J. S., Davidović, D., Reich, D. H. & Chien, C. L. Oscillatory superconducting transition temperature in Nb/Gd multilayers. *Phys. Rev. Lett.* **74**, 314–317 (1995).
- Ryazanov, V. V. *et al.* Coupling of two superconductors through a ferromagnet: Evidence for a  $\pi$  junction. *Phys. Rev. Lett.* **86**, 2427–2430 (2001).
- Kontos, T. *et al.* Josephson junction through a thin ferromagnetic layer: Negative coupling. *Phys. Rev. Lett.* **89**, 137007 (2002).
- Demler, E. A., Arnold, G. B. & Beasley, M. R. Superconducting proximity effects in magnetic metals. *Phys. Rev. B* **55**, 15174–15182 (1997).
- Bergeret, F. S., Volkov, A. F. & Efetov, K. B. Long-range proximity effects in superconductor–ferromagnet structures. *Phys. Rev. Lett.* **86**, 4096–4099 (2001).
- Kadigrobov, A., Shekhter, R. I. & Jonson, M. Quantum spin fluctuations as a source of long-range proximity effects in diffusive ferromagnet–superconductor structures. *Europhys. Lett.* **54**, 394–400 (2001).
- Eschrig, M., Kopu, J., Cuevas, J. C. & Schön, G. Theory of half-metal/superconductor heterostructures. *Phys. Rev. Lett.* **90**, 137003 (2003).
- Keizer, R. S. *et al.* A spin triplet supercurrent through the half-metallic ferromagnet CrO<sub>2</sub>. *Nature* **439**, 825–827 (2006).
- Robinson, J. W. A., Witt, J. D. S. & Blamire, M. G. Controlled injection of spin-triplet supercurrents into a strong ferromagnet. *Science* **329**, 59–61 (2010).
- Khaire, T. S., Khasawneh, M. A., Pratt, W. P. Jr & Birge, N. O. Observation of spin-triplet superconductivity in Co-based Josephson junctions. *Phys. Rev. Lett.* **104**, 137002 (2010).
- Bergeret, F. S., Volkov, A. F. & Efetov, K. B. Induced ferromagnetism due to superconductivity in superconductor–ferromagnet structures. *Phys. Rev. B* **69**, 174504 (2004).
- Löfwander, T., Champel, T., Durst, J. & Eschrig, M. Interplay of magnetic and superconducting proximity effects in ferromagnet–superconductor–ferromagnet trilayers. *Phys. Rev. Lett.* **95**, 187003 (2005).
- Pugach, N. G. & Buzdin, A. I. Magnetic moment manipulation by triplet Josephson current. *Appl. Phys. Lett.* **101**, 242602 (2012).
- Salikhov, R. I. *et al.* Experimental observation of the spin screening effect in superconductor/ferromagnet thin film heterostructures. *Phys. Rev. Lett.* **102**, 087003 (2009).
- Xia, J., Shelukhin, V., Karpovski, M., Kapitulnik, A. & Palevski, A. Inverse proximity effect in superconductor–ferromagnet bilayer structures. *Phys. Rev. Lett.* **102**, 087004 (2009).
- Khaydukov, Y. N. *et al.* On the feasibility to study inverse proximity effect in a single S/F bilayer by polarized neutron reflectometry. *JETP Lett.* **98**, 116–120 (2013).
- Flokstra, M. G. *et al.* Measurement of the spatial extent of inverse proximity in a Py/Nb/Py superconducting trilayer using low-energy muon-spin rotation. *Phys. Rev. B* **89**, 054510 (2014).
- Fominov, Y. V. *et al.* Superconducting triplet spin valve. *JETP Lett.* **91**, 308–313 (2010).
- Leksins, P. V. *et al.* Evidence for triplet superconductivity in a superconductor–ferromagnet spin valve. *Phys. Rev. Lett.* **109**, 057005 (2012).
- Zhu, L. Y. *et al.* Unanticipated proximity behavior in ferromagnet–superconductor heterostructures with controlled magnetic noncollinearity. *Phys. Rev. Lett.* **110**, 177001 (2013).



24. Flokstra, M. G. *et al.* Controlled suppression of superconductivity by the generation of polarized Cooper pairs in spin-valve structures. *Phys. Rev. B* **91**, 060501(R) (2015).
25. Bakule, P. & Morenzoni, E. Generation and applications of slow polarized muons. *Contemp. Phys.* **45**, 203–225 (2004).
26. Noh, T., Houzet, M., Meyer, J. S. & Chandrasekhar, V. Nonlocal spin correlations mediated by a superconductor. *Phys. Rev. B* **87**, 220502(R) (2013).
27. Sengupta, K. & Yakovenko, V. M. Spontaneous spin accumulation in singlet-triplet Josephson junctions. *Phys. Rev. Lett.* **101**, 187003 (2008).
28. Sears, M. R. & Saslow, W. M. Spin accumulation at ferromagnet/nonmagnetic material interfaces. *Phys. Rev. B* **85**, 014404 (2012).
29. Manchon, A., Ryzhanova, N., Vedyayev, A., Chschiev, M. & Dieny, B. Description of current-driven torques in magnetic tunnel junctions. *J. Phys. Condens. Matter* **20**, 145208 (2008).
30. Grein, R., Eschrig, M., Metalidis, G. & Schön, G. Spin-dependent Cooper pair phase and pure spin supercurrents in strongly polarized ferromagnets. *Phys. Rev. Lett.* **102**, 227005 (2009).
31. Alidoust, M., Linder, J., Rashedi, G., Yokoyama, T. & Sudbø, A. Spin-polarized Josephson current in superconductor/ferromagnet/superconductor junctions with inhomogeneous magnetization. *Phys. Rev. B* **81**, 014512 (2010).
32. Alidoust, M. & Halterman, K. Spontaneous edge accumulation of spin currents in finite-size two-dimensional diffusive spin-orbit coupled SFS heterostructures. *New J. Phys.* **17**, 033001 (2015).

## Acknowledgements

We acknowledge the support of the EPSRC through Grants No. EP/J01060X, No. EP/J010626/1, No. EP/J010650/1, No. EP/J010634/1 and No. EP/J010618/1, support of a studentship supported by JEOL Europe and the ISIS Neutron and Muon Source, and the support of the RFBR via awards No. 13-02-01452-a, No. 15-52-10045-Ko-a and No. 14-02-90018 Bel-a. All muon experiments were undertaken courtesy of the Paul Scherrer Institute. We thank J. M. Porro for assistance in acquiring the AFM images.

## Author contributions

J.K. and G.B. developed the samples; M.G.F., S.L.L., N.S., J.E.K.C., H.L. and T.P. performed the muon measurements, in which H.L., A.S. and T.P. provided the beamline support; M.G.F., S.L.L., N.S., J.E.K.C., P.J.C., S.J.B., C.J.K. and S.L. performed various support and characterization measurements; A.I., N.P. and M.E. provided theoretical interpretation of the data and helped writing the paper; G.B. and M.E. helped designing the study; M.G.F. and S.L.L. designed the study, analysed data and wrote the paper. All authors discussed the results and commented on the manuscript.

## Additional information

Supplementary information is available in the [online version of the paper](#). Reprints and permissions information is available online at [www.nature.com/reprints](http://www.nature.com/reprints). Correspondence and requests for materials should be addressed to M.G.F.

## Competing financial interests

The authors declare no competing financial interests.

## Methods

**Sample fabrication.** Samples were prepared by d.c. magnetron sputtering at a base pressure of  $10^{-8}$  mbar. Layers were grown *in situ* on Si(100) substrates at ambient temperature at a typical growth rate of  $0.2 \text{ nm s}^{-1}$ . The layout of our spin-valves is  $\text{Au}(x)/\text{Nb}(50)/\text{Co}(2.4)/\text{Nb}(3)/\text{Co}(1.2)/\text{IrMn}(4)/\text{Co}(3)/\text{Ta}(7.5)/\text{Si}$ -substrate with numbers giving the layer thickness in nm and  $x = 5$  or  $70$ . To obtain an ideal collinear arrangement in the  $\mu\text{SR}$  experiments, samples were also grown without the  $\text{IrMn}(4)/\text{Co}(3)$  pinning layer to ensure both F layers could be fully saturated and aligned with the field at  $150 \text{ G}$ . Growth was performed in the presence of a homogeneous magnetic field at the sample to establish the magnetic pinning of the Co layers adjacent to the IrMn, where the bottom Co layer is needed to set the initial direction for the IrMn to be pinned. The Ta buffer layer is to improve growth quality and the Au capping layer has a dual purpose. It protects the sample from oxidation and, depending on its thickness, allows the muons either to probe the Nb layer directly ( $5 \text{ nm Au cap}$ ) or to probe the observed proximity effect in the Au layer ( $70 \text{ nm Au cap}$ ).

**LE- $\mu\text{SR}$  measurements.** The low-energy muon spin-rotation (LE- $\mu\text{SR}$ ) experiments have been carried out at the  $\mu\text{E4}$ /low-energy muon (LEM)

beamline<sup>33</sup> of the Swiss Muon Source, as described in Supplementary Information 3.1. For all measurements the applied field was oriented in the sample plane, either perpendicular to the pinning direction (orthogonal arrangement) or aligned with the pinning direction (collinear arrangement). The field used to attain saturation of the free Co layer was  $150 \text{ G}$ . Temperature scans at fixed muon implantation energy were performed over a temperature range of  $3\text{--}20 \text{ K}$ , whereas energy scans were made both above  $T_c$  as well as below  $T_c$ . Typically  $2\text{--}6$  million muon decay events were counted for each muon experiment. The possibility of small thermal gradients across the sample was investigated by thermally grounding both the upper and lower surfaces of the sample to the sample plate, but was found to have no effect on any of the observations reported.

## References

33. Prokscha, T. *et al.* The new  $\mu\text{E4}$  beam at PSI: A hybrid-type large acceptance channel for the generation of a high intensity surface-muon beam. *Nucl. Instrum. Methods A* **595**, 317–331 (2008).